Comput Geosci (2013) 17:479–495
DOI 10.1007/s10596-013-9342-6

ORIGINAL PAPER

Ion transport in porous media: derivation of the macroscopic equations using upscaling and properties of the effective coefficients

Grégoire Allaire · Robert Brizzi · Jean-François Dufrêche · Andro Mikelić · Andrey Piatnitski

Received: 21 April 2012 / Accepted: 13 January 2013 / Published online: 26 February 2013

Abstract In this work, we undertake a numerical study of the effective coefficients arising in the upscaling of a system of partial differential equations describing transport of a dilute N-component electrolyte in a Newtonian solvent through a rigid porous medium. The motion is governed by a small static electric field and a small hydrodynamic force, around a nonlinear Poisson–Boltzmann equilibrium with given surface charges of arbitrary size. This approach allows us to calculate the linear response regime in a way initially proposed by O'Brien. The O'Brien linearization requires a fast and accurate solution of the underlying Poisson–Boltzmann equation. We present an analysis of it, with the discussion of the boundary layer appearing as the Debye–Hückel parameter becomes large. Next, we briefly discuss the corresponding two-scale asymptotic expansion and reduce the obtained two-scale equations to a coarse scale model. Our previous rigorous study proves that the homogenized coefficients satisfy Onsager properties, namely they are symmetric positive definite tensors. We illustrate with numerical simulations several characteristic situations and discuss the behavior of the effective coefficients when the Debye–Hückel parameter is large. Simulated qualitative behavior differs significantly from the situation when the surface potential is given (instead of the surface charges). In particular, we observe the Donnan effect (exclusion of co-ions for small pores).

Keywords Poisson–Boltzmann equation · Homogenization · Electroosmosis

G. Allaire (✉) · R. Brizzi
CMAP, UMR CNRS 7641, Ecole Polytechnique,
91128 Palaiseau Cedex, France
e-mail: gregoire.allaire@polytechnique.fr

R. Brizzi
e-mail: robert.brizzi@polytechnique.fr

J.-F Dufrêche
Laboratoire Modélisation Mésoscopique et Chimie Théorique (LMCT), Université de Montpellier 2,
Montpellier, France

J.-F Dufrêche
Institut de Chimie Séparative de Marcoule ICSM UMR 5257, CEA / CNRS / Université de Montpellier 2 / ENSCM
Centre de Marcoule, Bât. 426, BP 17171,
30207 Bagnols sur Cèze Cedex, France
e-mail: jean-francois.dufreche@univ-montp2.fr

A. Mikelić
Université de Lyon, CNRS UMR 5208, Université Lyon 1,
Institut Camille Jordan, 43, blvd. du 11 novembre 1918,
69622 Villeurbanne Cedex, France
e-mail: mikelic@univ-lyon1.fr

A. Piatnitski
Narvik University College, P.O. Box 385, 8505 Narvik,
Norway
e-mail: andrey@sci.lebedev.ru

A. Piatnitski
Lebedev Physical Institute RAS, Leninski ave., 53,
119991 Moscow, Russia

1 Introduction

The quasi-static transport of an electrolyte solution through an electrically charged porous medium is an important and well-known multi-scale problem in geosciences and porous materials modeling. An N-component electrolyte solution is a dilute solution of N species of charged particles, or ions, in a fluid which saturates a rigid porous medium. In such a case, the general solution is not simple because of the coupling between the electric field (created either by the internal charges or an external generator), the Stokes flow, and the convection–diffusion transport phenomena [27].

In fact, clays, and more generally numerous porous media are multi-scale materials. Thus, the description of the dynamics of such systems can be made at different scales. Hydrated smectite clays, such as montmorillonite, are lamellar mineral crystals composed of charged layers separated by an aqueous solution. They exhibit special features towards hydration and ion fixation [21]. Clay lamellae form thin platelet-shaped particles of diameter close to several hundreds of Angströms. But this lamellar geometry is valid only at small length scales. At larger scales, the structure is more complex and it leads to multi-porosities. Different modeling strategies are applied, depending on the size of the porosities. Ab initio molecular dynamics (see e.g., [6, 50]) provides information about the electronic degrees of freedom but, because of its computational cost, it is restricted to the smallest time and length scales. Classical Monte Carlo [48] or molecular dynamics simulations [15, 28] are able to describe larger systems. For example, the mechanism of crystalline swelling at low hydration is well reproduced by these techniques where the various atoms and ions are considered explicitly. Nevertheless, very large systems (e.g., for high hydration, or for macroporosities between different platelets particles) cannot be treated by this technique. The use of alternative methods based on continuous methods (e.g., Poisson–Boltzmann [49] descriptions or hydrodynamics [23, 44]) is inescapable. They are especially relevant for the derivation of the macroscopic law (such as Darcy's law) and for the calculation of the various electrokinetic phenomena.

These electrokinetic phenomena, such as the electroosmotic mechanism can facilitate or slow down fluid flowing through porous media. They are due to the *electric double layer* (EDL) which is formed as a result of the interaction of the ionized solution with static charges on the pore solid–liquid interface [19]. A part of the solute ions of opposite charge have a complex attraction with the surface and requires a specific treatment, forming the *Stern layer*. Its typical thickness is of one molecular diameter because of the molecular nature of the interface. After the Stern layer, the *electrostatic diffuse layer* or *Debye's layer* is formed, where the ion density varies smoothly, so that continuous models may be applied. The EDL is the union of Stern and diffuse layers. The thickness of the EDL is typically given by the Debye length λ_D, defined in the Debye–Hückel approach as the distance from the solid charged interface for which the solid charge is screened by the counterions. λ_D is typically a nanometric distance. Outside Debye's layer, in the remaining bulk fluid, the solvent can be considered as locally electrically neutral, because of the electrostatic screening. In the case of montmorillonite clays, the comparison with molecular dynamics simulations [13, 30] indicate that the Stern layer is globally negligible if the pore size is typically more than 1–2 nm. This is a consequence of the origin of the charge in these geological materials: clays are charged because of isomorphic substitutions so that the global charge is inside the volume of the solid phase and not at the surface. Thus, the surface Stern layer is less important.

The ion distribution in the EDL is characterized using the electrostatic potential Ψ. Its boundary value at the edge of Stern's layer characterizes the magnitude of the surface charge of the system. When measured by electrokinetic methods, for which the hydrodynamic no-slip surface is identified to the solid/fluid interface, it is known as the zeta potential ζ. This parameter is the one commonly used for the definition of the EDL. Yet it is an effective parameter, which depends on numerous parameters, such as the pH, the nature and the concentration of the electrolyte, and it is not defined rigorously for complex systems as clays for which the electric potential is not constant at the interface. In many situations, it is rather the surface charge density Σ, proportional to the normal derivative of Ψ, instead of ζ, which is relevant, because it corresponds to the chemistry of the system. In the case of montmorillonite clays, which is the case practically studied in this article, isomorphic substitutions give a bulk charge in the solid part, which can be modeled by a surface charge Σ [31] close to $1.61/2\ e.\mathrm{nm}^{-2}$.

Under the presence of an external electric field $\mathbf{E}$, the charged fluid may acquire a plug flow velocity which is proportional to $\mathbf{E}\zeta$ and given by the so-called Smoluchowski's formula. A more detailed, mathematically oriented, presentation of the fundamental concepts of electroosmotic flow in nanochannels can be found in the book [22] by Karniadakis et al., pages 447–470, from which we borrow the notations and definitions in this introduction.

In the case of porous media with large pores, the electroosmotic effects are modeled by introducing an effective slip velocity at the solid–liquid interfaces, which comes from the Smoluchowski formula. In this setting, the effective behavior of the charge transport through spatially periodic porous media was studied by Edwards in [14], using the volume averaging method.

On the other hand, in the case of clays, the characteristic pore size is also of the order of a few hundreds of nanometers or even less. Therefore, Debye's layer fills largely the pores, and its effect cannot anymore be modeled by an effective slip boundary condition at the liquid–solid interface. Furthermore, it was confirmed experimentally (see e.g., [9]) that the bulk Navier–Stokes equations still hold for pores larger than 1 nm. Therefore, in the present paper, we consider continuum equations at the microscopic level and, more precisely, we couple the incompressible Stokes equations for the fluid with the electrokinetic model made of a global electrostatic equation and one convection–diffusion equation for each type of ions.

The microscopic electrochemical interactions in an N-component electrolyte in a dilute Newtonian solvent are now well understood and in *SI units* we have in the stationary state the following mass conservation laws

$$\operatorname{div}\left(\mathbf{j}^i + \mathbf{u}n_i\right) = 0 \quad \text{in} \quad \Omega_p, \quad i = 1, \ldots, N, \tag{1}$$

where Ω_p is the pore space of the porous medium Ω. i denotes the solute species, $\mathbf{u}$ is the hydrodynamic velocity of solution, and n_i is the ith species concentration. Thus, $\mathbf{u}n_i$ is the convective flux for the species i while $\mathbf{j}^i$ is the migration-diffusion flux.

The hydrodynamic velocity is given by the Stokes equations, including the incompressibility condition,

$$\eta\Delta\mathbf{u} = \mathbf{f} + \nabla p + e\sum_{j=1}^{N} z_j n_j \nabla\Psi \qquad \text{in} \quad \Omega_p, \tag{2}$$

$$\operatorname{div}\mathbf{u} = 0 \qquad \text{in} \quad \Omega_p, \tag{3}$$

$$\mathbf{u} = 0 \qquad \text{on} \quad \partial\Omega_p \setminus \partial\Omega, \tag{4}$$

where η is the shear viscosity, $\mathbf{f}$ is the external body force, p is the pressure, e is the elementary charge, z_i is the charge number of the species i, and Ψ is the electrostatic potential. The pore boundary $\partial\Omega_p$ can be decomposed as the union of the fluid/solid boundaries $\partial\Omega_p \setminus \partial\Omega$, where we assume a no-slip boundary condition (4) and of the outer boundary $\partial\Omega$ of the porous medium Ω. In the case of clays [13, 30], this approach is valid even for nanometric porosities, because of the relatively low charge of the system. In fact, a slip boundary condition (with a slip length equal to a few Angströms) should be taken into account, but this microscopic slip will be neglected here (although it causes no special difficulties).

The migration–diffusion fluxes $\mathbf{j}^i$ are given by the following linear relationship

$$\mathbf{j}^i = \sum_{j=1}^{N} L_{ij} n_j\left(-\nabla\mu_j + z_j e\mathbf{E}\right),\ i = 1, \ldots, N;\ \mathbf{E} = -\nabla\Psi, \tag{5}$$

where μ_j is the chemical potential of the species j given by

$$\mu_j = \mu_j^0 + k_B T \ln n_j, \quad j = 1, \ldots, N, \tag{6}$$

where k_B is the Boltzmann constant, μ_j^0 is the standard chemical potential expressed at infinite dilution, and T is the absolute temperature. In Eq. 5, L_{ij} are the linear Onsager coefficients between the species j and i given, in this ideal model, by

$$L_{ij} = \frac{D_i^0}{k_B T}\delta_{ij}, \tag{7}$$

with δ_{ij} the Kronecker symbol. Furthermore, on the fluid/solid interfaces

$$\mathbf{j}^i \cdot \nu = 0 \quad \text{on} \quad \partial\Omega_p \setminus \partial\Omega, \quad i = 1, \ldots, N. \tag{8}$$

Our model is valid at infinite dilution, when the solution can be considered ideal, and D_i^0 is the diffusion coefficient of species i at infinite dilution. At finite concentration [12] these expressions, which correspond to the Poisson–Nernst–Planck equations, are not valid anymore. Here, we suppose that we are in the ideal case. Nonideal effects modify the ion transport and they will be studied in a forthcoming publication (Allaire et al., in preparation).

The electrostatic potential is calculated from the Poisson equation

$$\mathcal{E}\Delta\Psi = -e\sum_{j=1}^{N} z_j n_j \qquad \text{in} \quad \Omega_p, \tag{9}$$

where $\mathcal{E} = \mathcal{E}_0\mathcal{E}_r$ is the dielectric constant of the solvent. The corresponding boundary conditions is of Neumann type

$$\mathcal{E}\nabla\Psi \cdot \nu = -\Sigma \qquad \text{on} \quad \partial\Omega_p \setminus \partial\Omega, \tag{10}$$

where Σ is a given surface charge and ν is the unit exterior normal to Ω_p. We recall that Eq. 9 links the electrokinetic potential Ψ with the electric charge density $\rho_e = e\sum_{j=1}^{N} z_j n_j$. In the momentum Eq. 2, the elec-

Table 1 Data description

	Quantity	Values
e	Electron charge	1.6e−19 C (Coulomb)
D_i^0	Diffusivity of the ith species	$D_i^0 \in (1.79, 9.31)\text{e}{-09}\,\text{m}^2/\text{s}$
k_B	Boltzmann constant	1.38e−23 J/K
n_i	ith concentration	Number of particles/m^3
T	Temperature	293 K (Kelvin)
$\mathcal{E}$	Dielectric constant	6.93e−10 C/(mV)
η	Dynamic viscosity	$1\text{e}{-3}\,kg/(\text{m s})$
ℓ	Pore size	5e−9 m
λ_D	Debye's length	$\sqrt{\mathcal{E}k_BT/(\text{e}^2\text{n}_\text{c})} \in (3, 300)$ nm
z_j	jth electrolyte valence	Given integer
Σ	Surface charge density	$0.129C/\text{m}^2$ (clays)
$\mathbf{f}$	Given applied force	N/m^3
Ψ_c	Electrokinetic potential	0.02527 V (Volt)

trokinetic force per unit volume $\mathbf{f}_{EK} = \rho_e \nabla\Psi$ is taken into account. The boundary condition 8 means that the normal component of the ith species ionic flux, given by Eq. 5, vanishes at the pore boundaries. The various parameters appearing in Eqs. 1–10 are defined in Table 1.

For simplicity, we assume that $\Omega = (0, L)^d$ ($d = 2, 3$ is the space dimension) with $L > 0$. It remains to define the boundary conditions at the outer boundary $\partial\Omega$. Introducing an applied exterior potential $\Psi^{ext}(x)$, we impose periodic boundary conditions, in the sense that

$$\Psi + \Psi^{ext}(x)\ ,\ n_i\ ,\ \mathbf{u} \text{ and } P \text{ are } (0, L)^d - \text{periodic.} \quad (11)$$

Due to the complexity of the geometry and of the equations, it is necessary for engineering applications to upscale the system (Eqs. 1–11) and to replace the flow equations with a Darcy type law, including electroosmotic effects.

It is a common practice to assume that the porous medium is *statistically homogeneous*. A representative case is that of a periodic microstructure. Under such hypotheses, formal two-scale asymptotic expansion of the solutions of system (Eqs. 1–11) has been undertaken in many papers. Most of these works rely on a preliminary linearization of the problem which is first due to O'Brien et al. [37]. The earliest reference known to us, considering only one ionic species, is [4]. Detailed formal two-scale asymptotic expansion of the system (Eqs. 1–11), linearized in O'Brien's sense is due to Looker and Carnie in [26]. They obtained Onsager tensor but proved only its symmetry. The rigorous homogenization result is due to the authors in [3], where the positive definiteness of the Onsager tensor was proved too. Other contributions are due to Adler and his co-workers: [10] with a numerical study of the effective coefficients corresponding to the linearized equilibrium state, [29] with detailed calculations for the planar and circular Poiseuille pore flows, [1] with formulas for the effective coefficients in the random setting, [17] with a study of the behavior of the model in clay with small pores, [18] with the calculations of the effective coefficients for dense ball packing, and [43] where one find application to 1D clay sample.

Homogenization has also been studied for the fully nonlinear problem. Moyne and Murad considered the case of electroosmosis in deformable periodic porous media without linearization in the series of articles [32–36]. We mention in the same direction the work of Dormieux et al. [11]. More recent works on this topic are [40–42, 46] and [47].

The goal of the present paper is to numerically study the upscaling of a suitably scaled version of the above Eqs. 1–11, describing the transport of a dilute N-component electrolyte in a rigid periodic porous medium. We first briefly recall the effective equations obtained by rigorous homogenization in [3] (identical to those in [26]), as well as some asymptotics of the Poisson–Boltzmann equation for small and large pores, proved in [2]. Then, we compute the resulting effective tensors through the solutions of cell problems. In particular, we study their dependence on various parameters such as porosity and concentration.

In Section 2, we present the adimensionalization of the equations, followed by their partial linearization, in the spirit of the seminal work of O'Brien et al. [37]. This allows us to write the microscopic ε-problem in a periodic geometry. We further describe some qualitative properties of the nonlinear Poisson–Boltzmann equation at the equilibrium state when the pore size is small or large compared to the Debye length. In Section 3, we present the results of the two-scale asymptotic expansion method, allowing to homogenize or upscale the microscopic ε-problem. We discuss the linear relation linking the ionic current, filtration velocity, and ionic fluxes with gradients of the electrical potential, pressure, and ionic concentrations. More precisely, in Proposition 5, we recall that the so-called Onsager relations [16] are satisfied, namely the full homogenized tensor is symmetric positive definite. Finally, in Section 4, we present a numerical study of the obtained homogenized coefficients, including their sensitivities to various physical parameters. Since, for simplicity reasons, we content ourselves with 2-d numerical simulations, we cannot use realistic microstructures, corresponding to montmorillonite clays. We therefore perform our computations on artificial plane microgeometries which are easily parameterized to take into account varying porosities or pore size.

2 Nondimensional form and linearization

2.1 The nondimensional form

Before any asymptotic analysis, we need a dimensionless form of the Eqs. 1–3, 5, 6, 9, and 10. We first note that the known data are the characteristic pore size ℓ, the surface charge density $\Sigma(x)$ (having the characteristic value Σ_c), the static electrical potential Ψ^{ext}, and the applied fluid force $\mathbf{f}$. The small parameter is $\varepsilon = \dfrac{\ell}{L} << 1$; the ratio between the pore size and the dimension of the porous medium.

We proceed differently than in [22] and [26]. We are interested in characteristic concentrations n_c taking values in the range $(10^{-2}, 1)$ mol/l, i.e., (6.022e24, 6.022e26) m^{-3}. Using the definition of Debye's length from Table 1

$$\lambda_D = \sqrt{\frac{\mathcal{E} k_B T}{e^2 n_c}},$$

we find out that $\lambda_D \in (0.042, 0.42)$ nm.

Next, following the nondimensionalization from [22], we introduce the characteristic potential $\zeta = k_B T/e$ and the parameter β related to the Debye–Hückel parameter $\kappa = 1/\lambda_D$, as follows

$$\beta = \left(\frac{\ell}{\lambda_D}\right)^2. \tag{12}$$

The parameter β is the fundamental physical characteristics which drives the transport properties of an electrolyte solution in a porous media. For large β the electrical potential is concentrated in a diffuse layer next to the liquid/solid interface. Co-ions, for which the charge is the same as the one of the solid phase are able to go everywhere in the porosities because the repelling electrostatic force of the solid phase is screened by the counterions. The electrostatic phenomena are mainly surficial, and the interfaces are globally independent. For small β, co-ions do not have access to the very small porosities (Donnan effect). The local electroneutrality condition is not valid anymore and the electric fields of the solid interfaces are coupled.

Next, we rescale the space variable by setting $\Omega^\varepsilon = \Omega_p/L$ and $x' = \frac{x}{L}$ (we shall drop the primes for simplicity in the sequel). We introduce other characteristic quantities

$$p_c = n_c k_B T, \quad u_c = \varepsilon^2 \frac{k_B T n_c L}{\eta},$$

adimensionalized forcing terms

$$\Psi^{ext,*} = \frac{e\Psi^{ext}}{k_B T}, \quad \mathbf{f}^* = \frac{\mathbf{f} L}{p_c}, \quad \Sigma^* = \frac{\Sigma}{\Sigma_c}, \quad N_\sigma = \frac{e\Sigma_c \ell}{\mathcal{E} k_B T},$$

and adimensionalized unknowns

$$p^\varepsilon = \frac{p}{p_c}, \ \mathbf{u}^\varepsilon = \frac{\mathbf{u}}{u_c}, \ \Psi^\varepsilon = \frac{e\Psi}{k_B T}, \ n_j^\varepsilon = \frac{n_j}{n_c}.$$

Remark that $N_\sigma = \ell/L_G$, where L_G is the Gouy length. With our numerical values we find out that $N_\sigma \approx 36.83$. The assumption $N_\sigma = \mathcal{O}(1)$ is classical in the literature [26] and [32]. Concerning the transport term, we easily find out that the global Peclet number for the jth species Pe_j is

$$\mathrm{Pe}_j = \frac{u_c L}{D_j^0} = \frac{\ell^2 k_B T n_c}{\eta D_j^0} \in (0.01085, 1.085).$$

We are now in a situation to write the dimensionless equations for hydrodynamic and electrostatic parts:

$$\varepsilon^2 \Delta \mathbf{u}^\varepsilon - \nabla p^\varepsilon = \mathbf{f}^* + \sum_{j=1}^{N} z_j n_j^\varepsilon(x) \nabla \Psi^\varepsilon \ \text{ in } \Omega^\varepsilon, \tag{13}$$

$$\mathbf{u}^\varepsilon = 0 \ \text{ on } \partial\Omega^\varepsilon \setminus \partial\Omega, \quad \text{div } \mathbf{u}^\varepsilon = 0 \quad \text{in } \Omega^\varepsilon, \tag{14}$$

$$-\varepsilon^2 \Delta \Psi^\varepsilon = \beta \sum_{j=1}^{N} z_j n_j^\varepsilon(x) \quad \text{in } \Omega^\varepsilon; \tag{15}$$

$$\varepsilon \nabla \Psi^\varepsilon \cdot \nu = -N_\sigma \Sigma^* \ \text{ on } \partial\Omega^\varepsilon \setminus \partial\Omega, \tag{16}$$

$$\text{div}\left(n_j^\varepsilon \nabla \ln(n_j^\varepsilon e^{\Psi^\varepsilon z_j}) - \mathrm{Pe}_j n_j^\varepsilon \mathbf{u}^\varepsilon\right) = 0 \ \text{ in } \Omega^\varepsilon, \tag{17}$$

$$\nabla \ln(n_j^\varepsilon e^{\Psi^\varepsilon z_j}) \cdot \nu = 0 \ \text{ on } \partial\Omega^\varepsilon \setminus \partial\Omega, \tag{18}$$

$$n_j^\varepsilon, \ (\Psi^\varepsilon + \Psi^{ext,*}), \ \mathbf{u}^\varepsilon \ \text{ and } \ p^\varepsilon \quad \text{are } 1-\text{periodic in } x. \tag{19}$$

For simplicity, in the sequel, we denote by $\mathbf{E}^*$ the imposed electric field corresponding to the exterior potential $\Psi^{ext,*}$, i.e., $\mathbf{E}^*(x) = \nabla \Psi^{ext,*}(x)$.

2.2 Linearization

The applied source terms in system (Eqs. 13–19) are the static electric potential $\Psi^{ext,*}(x)$, the surface charge density $N_\sigma \Sigma^*(x)$ on the pore walls, and the applied

fluid force $\mathbf{f}^*(x)$. The fields $\mathbf{f}^*$ and $\Psi^{ext,*}$ are assumed to be sufficiently small to allow the partial linearization of the ionic transport (electrokinetic) equations. No smallness condition is imposed on $N_\sigma \Sigma^*$, and the Poisson–Boltzmann equation remains nonlinear.

Following the calculations by O'Brien et al. from the seminal paper [37], we write the electrokinetic unknowns as

$$n_i^\varepsilon(x) = n_i^{0,\varepsilon}(x) + \delta n_i^\varepsilon(x), \quad \Psi^\varepsilon(x) = \Psi^{0,\varepsilon}(x) + \delta\Psi^\varepsilon(x),$$
$$\mathbf{u}^\varepsilon(x) = \mathbf{u}^{0,\varepsilon}(x) + \delta\mathbf{u}^\varepsilon(x), \quad p^\varepsilon(x) = p^{0,\varepsilon}(x) + \delta p^\varepsilon(x),$$

where $n_i^{0,\varepsilon}$, $\Psi^{0,\varepsilon}$, $\mathbf{u}^{0,\varepsilon}$, and $p^{0,\varepsilon}$ are the equilibrium quantities, corresponding to $\mathbf{f}^* = 0$ and $\Psi^{ext,*} = 0$. The δ prefix indicates a perturbation.

In the case $\mathbf{f}^* = 0$ and $\Psi^{ext,*} = 0$, one can find a special solution of Eqs. 13–19 by assuming that the fluid is at rest and the flux in Eq. 17 is zero everywhere. It is given by

$$\mathbf{u}^{0,\varepsilon} = 0\,, \quad p^{0,\varepsilon} = \sum_{j=1}^{N} n_j^c \exp\{-z_j\Psi^{0,\varepsilon}\}\,,$$
$$n_j^{0,\varepsilon}(x) = n_j^c \exp\{-z_j\Psi^{0,\varepsilon}(x)\}\,, \tag{20}$$

where $\Psi^{0,\varepsilon}$ is a solution of the Poisson–Boltzmann equation

$$\begin{cases} -\varepsilon^2\Delta\Psi^{0,\varepsilon} = \beta\displaystyle\sum_{j=1}^{N} z_j n_j^c e^{-z_j\Psi^{0,\varepsilon}} \text{ in } \Omega^\varepsilon, \\ \varepsilon\nabla\Psi^{0,\varepsilon}\cdot\nu = -N_\sigma\Sigma^* \text{ on } S_\varepsilon = \partial\Omega^\varepsilon \setminus \partial\Omega, \\ \Psi^{0,\varepsilon} \text{ is } 1-\text{periodic}. \end{cases} \tag{21}$$

The constants $n_j^c > 0$ are called the infinite dilution concentrations. We note that problem 21 is equivalent to the following minimization problem:

$$\inf_{\varphi\in V_\varepsilon} J_\varepsilon(\varphi), \tag{22}$$

with $V_\varepsilon = \{\varphi \in H^1(\Omega^\varepsilon),\ \varphi \text{ is } 1-\text{periodic}\}$ and

$$J_\varepsilon(\varphi) = \frac{\varepsilon^2}{2}\int_{\Omega_\varepsilon} |\nabla\varphi|^2\, dx + \beta\sum_{j=1}^{N}\int_{\Omega_\varepsilon} n_j^c e^{-z_j\varphi}\, dx + \varepsilon N_\sigma\int_{S_\varepsilon}\Sigma^*\varphi\, dS.$$

The functional J_ε is strictly convex, which gives the uniqueness of the minimizer. Nevertheless, for arbitrary nonnegative β, n_j^c and N_σ, J_ε may be *not coercive* on V_ε if all z_j's have the same sign (take φ to be constant, of the same sign as the z_j's and going to infinity). Therefore, we must put a condition on the z_j so that the minimization problem 22 admits a solution. Following the literature, we impose the *bulk electroneutrality condition*

$$\sum_{j=1}^{N} z_j n_j^c = 0, \tag{23}$$

which guarantees that for $\Sigma^* = 0$, the unique solution is $\Psi^{0,\varepsilon} = 0$. Under Eq. 23, it is easy to see that J_ε is coercive on V_ε.

Remark 1 The bulk electroneutrality condition 23 is not a restriction. Actually, all our results hold under the much weaker assumption that all valences z_j do not have the same sign. Indeed, if Eq. 23 is not satisfied, we can make a change of variables in the Poisson–Boltzmann Eq. 21, defining a new potential $\tilde{\Psi}^{0,\varepsilon} = \Psi^{0,\varepsilon} + \Psi^C$, where Ψ^C is a constant reference potential. Since the function

$$\Psi^C \to -\sum_{j=1}^{N} z_j n_j^c e^{-z_j\Psi^C}$$

is continuous, increasing, and admits the limits $\pm\infty$ as Ψ^C goes to $\pm\infty$, there exists a unique root Ψ^C of this function. This change of variables for the potential leaves (Eq. 21) invariant if we change the constants n_j^c in new constants $\tilde{n}_j^c = n_j^c e^{-z_j\Psi^C}$. These new constants satisfy the bulk electroneutrality condition 23.

Lemma 2 [25] *Assume that the electroneutrality condition 23 holds true and Σ^* be a smooth bounded function. Then problem 22 has a unique solution $\Psi^{0,\varepsilon} \in V_\varepsilon$.*

Motivated by the form of the Boltzmann equilibrium distribution and the calculation of $n_i^{0,\varepsilon}$, we follow the lead of [37] and introduce the so-called ionic potential Φ_i^ε which is defined in terms of n_i^ε by

$$n_i^\varepsilon = n_i^c \exp\{-z_i(\Psi^\varepsilon + \Phi_i^\varepsilon + \Psi^{ext,*})\}. \tag{24}$$

After linearization, Eq. 24 leads to

$$\delta n_i^\varepsilon(x) = -z_i n_i^{0,\varepsilon}(x)(\delta\Psi^\varepsilon(x) + \Phi_i^\varepsilon(x) + \Psi^{ext,*}(x)). \tag{25}$$

Introducing Eq. 25 into Eqs. 13–17 and linearizing yields the following equations

$$\varepsilon^2\Delta\mathbf{u}^\varepsilon - \nabla P^\varepsilon = \mathbf{f}^* - \sum_{j=1}^{N} z_j n_j^{0,\varepsilon}(x)(\nabla\Phi_j^\varepsilon + \mathbf{E}^*) \text{ in } \Omega^\varepsilon, \tag{26}$$

$$\operatorname{div} \mathbf{u}^\varepsilon = 0 \ \text{ in } \Omega^\varepsilon, \quad \mathbf{u}^\varepsilon = 0 \ \text{ on } \partial\Omega^\varepsilon \setminus \partial\Omega, \tag{27}$$

$$\operatorname{div}\left(n_j^{0,\varepsilon}(x)\left(\nabla\Phi_j^\varepsilon + \mathbf{E}^* + \frac{\mathrm{Pe}_j}{z_j}\mathbf{u}^\varepsilon\right)\right) = 0 \ \text{ in } \Omega^\varepsilon, \tag{28}$$

$$(\nabla\Phi_j^\varepsilon + \mathbf{E}^*)\cdot\nu = 0 \ \text{ on } \partial\Omega^\varepsilon \setminus \partial\Omega, \tag{29}$$

$$\mathbf{u}^\varepsilon,\ P^\varepsilon,\ \Phi_j^\varepsilon \ \text{ are } 1-\text{periodic}, \tag{30}$$

where the perturbed velocity is actually equal to the overall velocity and, for convenience, we introduced a global pressure P^ε

$$\delta\mathbf{u}^\varepsilon = \mathbf{u}^\varepsilon, \quad P^\varepsilon = \delta p^\varepsilon + \sum_{j=1}^N z_j n_j^{0,\varepsilon}\left(\delta\Psi^\varepsilon + \Phi_j^\varepsilon + \Psi^{ext,*}\right). \tag{31}$$

It is important to remark that, after the global pressure P^ε has been introduced, $\delta\Psi^\varepsilon$ does not enter Eqs. 26–30 and thus is decoupled from the main unknowns $\mathbf{u}^\varepsilon$, P^ε and Φ_i^ε. The system (Eqs. 20, 21, 26–30) is the same microscopic linearized system for the ionic transport as in the papers by Adler et al. [1, 10, 17, 29, 43] and in the work of Looker and Carnie [26].

2.3 Poisson–Boltzmann equation in the periodicity cell

It is now time to make precise the geometrical structure of the porous medium. From now on, we assume that Ω^ε is an ε-periodic open subset of $\mathbb{R}^d$. It is built from $(0,1)^d$ by removing a periodic distributions of solid obstacles which, after rescaling, are all similar to the unit obstacle Y_S. More precisely, we consider a smooth partition of the unit periodicity cell $Y = Y_S \cup Y_F$, where Y_S is the solid part and Y_F is the fluid part. The liquid/solid interface is $S = \partial Y_S \setminus \partial Y$. The fluid part is assumed to be a smooth connected open subset (no assumption is made on the solid part). We define $Y_\varepsilon^j = \varepsilon(Y_F + j)$, $S_\varepsilon^j = \varepsilon(S + j)$, $\Omega^\varepsilon = \bigcup_{j\in\mathbb{Z}^d} Y_\varepsilon^j \cap \Omega$, and $S_\varepsilon \equiv \partial\Omega^\varepsilon \setminus \partial\Omega = \bigcup_{j\in\mathbb{Z}^d} S_\varepsilon^j \cap \Omega$.

We also assume a periodic distribution of charges $\Sigma^* \equiv \Sigma^*(x/\varepsilon)$. Then, by periodicity of Ω^ε and by uniqueness of the solution $\Psi^{0,\varepsilon}$ of the Poisson–Boltzmann Eq. 21, we have

$$\Psi^{0,\varepsilon}(x) = \Psi^0\left(\frac{x}{\varepsilon}\right), \quad n_j^{0,\varepsilon}(x) = n_j^0\left(\frac{x}{\varepsilon}\right), \tag{32}$$

where

$$n_j^0(y) = n_j^c \exp\{-z_j\Psi^0(y)\} \tag{33}$$

and $\Psi^0(y)$ is the periodic solution for the cell Poisson–Boltzmann equation

$$\begin{cases} -\Delta\Psi^0 = \beta\displaystyle\sum_{j=1}^N z_j n_j^c e^{-z_j\Psi^0} \ \text{ in } \ Y_F, \\ \nabla\Psi^0\cdot\nu = -N_\sigma\Sigma^* \ \text{ on } \ S, \\ \Psi^0 \ \text{ is } 1-\text{periodic}. \end{cases} \tag{34}$$

Solvability of Eq. 34 is again a consequence of Lemma 2 and of the electroneutrality condition 23.

We now briefly describe the asymptotic behavior of the solution $\Psi^0(y)$ of Eq. 34 for large and small β. A rigorous and more complete analysis is done in our other paper [2]. Similar asymptotic analysis have been performed in [5, 38]. Note that, in Eq. 34, the parameter β is a multiplier of the infinite dilution concentrations n_j^c. Therefore, studying large or small values of β is equivalent to study large or small common values of the n_j^c's. In view of its definition (Eq. 12), a large value of β corresponds either to a large pore size or to a small Debye length.

When β goes to $+\infty$, simple asymptotic analysis argument, using an outer two-scale expansion, guarantees that $\Psi^0(y)$ behaves as a constant which is the root of the nonlinearity in the Poisson–Boltzmann equation. By the electroneutrality condition 23, this unique root is zero. Hence, we deduce

$$\Psi^0(y) = O\left(\frac{1}{\beta}\right) \ \text{ in } Y_F, \text{ away from the boundary } \ S. \tag{35}$$

The behavior of Ψ^0 in the vicinity of the boundary S is given by a boundary layer which is exponentially decaying away from S as $\exp\{-d(y)/\beta\}$ where $d(y)$ is the distance function to S (a precise description is given in [2]).

When β goes to 0 (very small pores), the asymptotic analysis is less trivial and reveals the so-called Donnan effect (co-ions do not have access to the very small porosities). The variational formulation of Eq. 34 is

$$\int_{Y_F} \nabla\Psi^0 \cdot \nabla\varphi\, dy - \beta\int_{Y_F}\sum_{j=1}^N z_j n_j^c e^{-z_j\Psi^0}\varphi\, dy + \int_S N_\sigma\Sigma^*\varphi\, dS = 0, \tag{36}$$

for any smooth 1-periodic test function φ. If we choose $\varphi = 1$ in Eq. 36, then we get

$$\int_{Y_F}\sum_{j=1}^N z_j n_j^c e^{-z_j\Psi^0}\, dy = \beta^{-1}\int_S N_\sigma\Sigma^*\, dS. \tag{37}$$

Thus, $\int_S \Sigma^* \, dS \neq 0$ implies that the left hand side of Eq. 37 blows up as β goes to zero, which means that the function Ψ^0 cannot stay bounded. Nevertheless, it turns out that the function $\Psi^0 - \frac{1}{|Y_F|}\int_{Y_F} \Psi^0 \, dy$ remains bounded. We have three cases.

Case 1: $\int_S \Sigma^* < 0$. In this case, it is the negative valence with maximum value, $z^- = \max_j(-z_j) > 0$, which matters. We obtain

$$\Psi^0(y) = \frac{1}{z^-}\log\left(\frac{1}{\beta}\right) + \varphi_0(y) + O(\beta^{1/z^-}), \tag{38}$$

and φ_0 is the solution to the boundary value problem

$$\begin{cases} -\Delta\varphi_0(y) + z^- n_-^c e^{z^-\varphi_0(y)} = 0 \text{ in } Y_F, \\ \nabla\varphi_0 \cdot \nu = -N_\sigma \Sigma^* \text{ on } S, \\ \varphi_0 \text{ is } 1-\text{periodic}, \end{cases} \tag{39}$$

with $n_-^c = n_j^c$ for j such that $z^- = -z_j$. All other species are negligible, $n_j^c << n_-^c$ for j such that $z^- \neq -z_j$, and in particular the concentration of co-ions (of the same valence than the surface charge) is asymptotically vanishing (Donnan effect). We note that Eq. 39 is solvable only for $\int_S \Sigma^* < 0$.

Case 2: $\int_S \Sigma^* > 0$. In this case, it is the positive valence with maximum value, $z^+ = \max_j z_j > 0$, which matters (here again, all other species are negligible). We obtain

$$\Psi_\beta(y) = -\frac{1}{z^+}\log\left(\frac{1}{\beta}\right) + \xi_0(y) + O(\beta^{1/z^+}), \tag{40}$$

where ξ_0 is the solution to the boundary value problem

$$\begin{cases} -\Delta\xi_0(y) - z^+ n_+^c e^{-z^+\xi_0(y)} = 0 \text{ in } Y_F, \\ \nabla\xi_0 \cdot \nu = -N_\sigma \Sigma^* \text{ on } S, \\ \xi_0 \text{ is } 1-\text{periodic}. \end{cases} \tag{41}$$

Again, Eq. 41 is solvable only for $\int_S \Sigma^* > 0$.

Case 3: $\int_S \Sigma^* = 0$. In this case, things are much simpler. Let Ψ_{N0} be the unique solution, such that $\int_{Y_F} \sum_{j=1}^N z_j n_j^c e^{-z_j\Psi_{N0}} \, dy = 0$, of

$$\begin{cases} -\Delta\Psi_{N0}(y) = 0 \text{ in } Y_F, \\ \nabla\Psi_{N0} \cdot \nu = -N_\sigma \Sigma^* \text{ on } S, \\ \Psi_{N0} \text{ is } 1-\text{periodic}. \end{cases} \tag{42}$$

Then we have

$$\Psi^0(y) = \Psi_{N0}(y) + O(\beta). \tag{43}$$

Note that the solutions of Eq. 42 are defined up to an additive constant which is determined, in the present case, by the additional average condition.

3 Homogenization

After solving the nonlinear Poisson–Boltzmann equation, which yields the equilibrium concentrations $n_j^{0,\varepsilon}(x)$, the problem to homogenize is the system of linearized Eqs. 26–30, where $n_j^{0,\varepsilon}(x)$ are ε-periodic coefficients defined by Eqs. 20 and 32.

The formal two-scale asymptotic expansion method [7, 20, 45] was applied to system 26–30 in [26]. It is also a special case of more general expansions in [32–34, 36]. Introducing the fast variable $y = x/\varepsilon$, it is assumed that the solution of Eqs. 26–30 is given by

$$\begin{cases} \mathbf{u}^\varepsilon(x) = \mathbf{u}^0(x,y) + \varepsilon\mathbf{u}^1(x,y) + \ldots, \\ P^\varepsilon(x) = p^0(x) + \varepsilon p^1(x,y) + \ldots, \\ \Psi^\varepsilon(x) = \Psi^0(x,y) + \varepsilon\Psi^1(x,y) + \ldots, \\ \Phi_j^\varepsilon(x) = \Phi_j^0(x) + \varepsilon\Phi_j^1(x,y) + \ldots. \end{cases}$$

After some calculations [26], we obtain the following two-scale homogenized problem.

Theorem 3 *$(\mathbf{u}^0, p^0, p^1, \{\Phi_j^0, \Phi_j^1\})$ is the unique solution of the two-scale homogenized problem*

$$-\Delta_y \mathbf{u}^0(x,y) + \nabla_y p^1(x,y) = -\nabla_x p^0(x) - \mathbf{f}^*(x)$$

$$+\sum_{j=1}^N z_j n_j^0(y)(\nabla_x\Phi_j^0(x) + \nabla_y\Phi_j^1(x,y) + \mathbf{E}^*(x)) \text{ in } \Omega\times Y_F, \tag{44}$$

$$\operatorname{div}_y \mathbf{u}^0(x,y) = 0 \text{ in } \Omega\times Y_F, \ \mathbf{u}^0(x,y) = 0 \text{ on } \Omega\times S, \tag{45}$$

$$\mathrm{div}_x\left(\int_{Y_F}\mathbf{u}^0\,dy\right)=0\ \ in\ \Omega, \tag{46}$$

$$-\mathrm{div}_y\left(n_j^0(y)\left(\nabla_y\Phi_j^1(x,y)+\nabla_x\Phi_j^0(x)+\mathbf{E}^*(x)+\frac{\mathrm{Pe}_j}{z_j}\mathbf{u}^0\right)\right)=0\ \ in\ \Omega\times Y_F, \tag{47}$$

$$\left(\nabla_y\Phi_j^1+\nabla_x\Phi_j^0+\mathbf{E}^*\right)\cdot\nu(y)=0\ \ on\ \Omega\times S, \tag{48}$$

$$-\mathrm{div}_x\left(\int_{Y_F}n_j^0\left(\nabla_y\Phi_j^1+\nabla_x\Phi_j^0+\mathbf{E}^*(x)+\frac{\mathrm{Pe}_j}{z_j}\mathbf{u}^0\right)dy\right)=0\ in\ \Omega, \tag{49}$$

$$\Phi_j^0\,,\ \int_{Y_F}\mathbf{u}^0\,dy\ \ and\ \ p^0\ being\ 1\text{-}periodic\ in\ x, \tag{50}$$

with periodic boundary conditions on the unit cell Y_F for all functions depending on y.

The limit problem introduced in Theorem 3 is called the two-scale and two-pressure homogenized problem, following the terminology of [20, 24]. It is well posed [3] because the two incompressibility constraints 45 and 46 are exactly dual to the two pressures $p^0(x)$ and $p^1(x,y)$ which are their corresponding Lagrange multipliers.

Of course, one should extract from Eqs. 44–50 the macroscopic homogenized problem, which requires to separate the fast and slow scale, if possible. This was undertaken by Looker and Carnie in [26] introducing three different types of cell problems. In [3], we simplified their analysis by proposing only two types of cell problems. Our approach was also more systematic because it allowed us to establish Onsager properties for the effective coefficients. We repeat the scale separation results in order to be able to establish further qualitative properties of the effective coefficients and to state the convergence result.

The main idea is to recognize in the two-scale homogenized problem (Eqs. 44–50) that there are two different macroscopic fluxes, namely $(\nabla_x p^0(x)+\mathbf{f}^*(x))$ and $\{\nabla_x\Phi_j^0(x)+\mathbf{E}^*(x)\}_{1\le j\le N}$. Therefore, we introduce two family of cell problems, indexed by $k\in\{1,...,d\}$ for each component of these fluxes. We denote by $\{\mathbf{e}^k\}_{1\le k\le d}$ the canonical basis of $\mathbb{R}^d$.

The first cell problem, corresponding to the macroscopic pressure gradient, is

$$-\Delta_y\mathbf{v}^{0,k}(y)+\nabla_y\pi^{0,k}(y)=\mathbf{e}^k+\sum_{j=1}^N z_j n_j^0(y)\nabla_y\theta_j^{0,k}(y)\ \ \text{in } Y_F \tag{51}$$

$$\mathrm{div}_y\,\mathbf{v}^{0,k}(y)=0\quad \text{in } Y_F,\quad \mathbf{v}^{0,k}(y)=0\ \text{on } S, \tag{52}$$

$$-\mathrm{div}_y\left(n_j^0(y)\left(\nabla_y\theta_j^{0,k}(y)+\frac{\mathrm{Pe}_j}{z_j}\mathbf{v}^{0,k}(y)\right)\right)=0\ \text{ in } Y_F \tag{53}$$

$$\nabla_y\theta_j^{0,k}(y)\cdot\nu=0\ \text{ on } S. \tag{54}$$

The second cell problem, corresponding to the macroscopic diffusive flux, is for each species $i\in\{1,...,N\}$

$$-\Delta_y\mathbf{v}^{i,k}(y)+\nabla_y\pi^{i,k}(y)=\sum_{j=1}^N z_j n_j^0(y)(\delta_{ij}\mathbf{e}^k+\nabla_y\theta_j^{i,k}(y))\ \text{ in } Y_F \tag{55}$$

$$\mathrm{div}_y\,\mathbf{v}^{i,k}(y)=0\quad \text{in } Y_F,\quad \mathbf{v}^{i,k}(y)=0\quad \text{on } S, \tag{56}$$

$$-\mathrm{div}_y\left(n_j^0(y)\left(\delta_{ij}\mathbf{e}^k+\nabla_y\theta_j^{i,k}(y)+\frac{\mathrm{Pe}_j}{z_j}\mathbf{v}^{i,k}(y)\right)\right)=0\ \text{ in } Y_F \tag{57}$$

$$\left(\delta_{ij}\mathbf{e}^k+\nabla_y\theta_j^{i,k}(y)\right)\cdot\nu=0\ \text{ on } S, \tag{58}$$

where δ_{ij} is the Kronecker symbol. As usual, the cell problems are complemented with periodic boundary conditions.

Remark 4 For β going to $+\infty$, we know from Eq. 35 that the potential $\Psi^0(y)\equiv 0$ and thus, from Eq. 33, we deduce that $n_j^0(y)\equiv n_j^c$ are constant in the cell Y_F. Obviously, it implies that the solution $\theta_j^{0,k}(y)$ of Eqs. 53 and 54 is a constant too and the solution $(\pi^{0,k},\mathbf{v}^{0,k})$ of Eqs. 51 and 52 is identical to the solution of the classic permeability problem [20, 45]. Similarly, upon defining a new pressure $\pi^{i,k}-\sum_{j=1}^N z_j n_j^c\theta_j^{i,k}$, the solution $(\pi^{i,k},\mathbf{v}^{i,k})$ of Eqs. 55 and 56 is identical to the solution of the classic permeability problem in the limit $\beta\to+\infty$, while the solution $\theta_j^{i,k}(y)$ of Eqs. 57 and

58 coincides with the cell solution for the Neumann problem in a perforated domain [45].

As already explained in Section 2.3, as far as the behavior of the Poisson–Boltzmann equation is concerned, the limit β going to $+\infty$ is equivalent to the limit of a common value of all infinite dilution concentrations n_j^c going to $+\infty$. The same is true for the above cell problems upon redefining the pressure (which may be unbounded as n_j^c grows), except for the velocity $\mathbf{v}^{i,k}$, solution of Eqs. 55 and 56, which grows linearly with n_j^c and is such that $\mathbf{v}^{i,k}/n_j^c$ converges to the usual velocity for a classic permeability problem.

Then, we can decompose the solution of Eqs. 44–50 as

$$\mathbf{u}^0(x,y) = \sum_{k=1}^{d}\left(-\mathbf{v}^{0,k}(y)\left(\frac{\partial p^0}{\partial x_k} + f_k^*\right)(x) + \sum_{i=1}^{N}\mathbf{v}^{i,k}(y)\left(E_k^* + \frac{\partial \Phi_i^0}{\partial x_k}\right)(x)\right) \tag{59}$$

$$p^1(x,y) = \sum_{k=1}^{d}\left(-\pi^{0,k}(y)\left(\frac{\partial p^0}{\partial x_k} + f_k^*\right)(x) + \sum_{i=1}^{N}\pi^{i,k}(y)\left(E_k^* + \frac{\partial \Phi_i^0}{\partial x_k}\right)(x)\right) \tag{60}$$

$$\Phi_j^1(x,y) = \sum_{k=1}^{d}\left(-\theta_j^{0,k}(y)\left(\frac{\partial p^0}{\partial x_k} + f_k^*\right)(x) + \sum_{i=1}^{N}\theta_j^{i,k}(y)\left(E_k^* + \frac{\partial \Phi_i^0}{\partial x_k}\right)(x)\right). \tag{61}$$

We average Eqs. 59–61 in order to get a purely macroscopic homogenized problem. We introduce the nondimensional perturbation of the electrochemical potential

$$\delta\mu_j^\varepsilon = -z_j(\Phi_j^\varepsilon + \Psi^{ext,*})$$

and the ionic flux of the jth species

$$\mathbf{j}_j^\varepsilon = \frac{z_j}{\mathrm{Pe}_j} n_j^\varepsilon\left(\nabla\Phi_j^\varepsilon + \mathbf{E}^* + \frac{\mathrm{Pe}_j}{z_j}\mathbf{u}^\varepsilon\right).$$

We define the homogenized quantities

$$\mu_j(x) = -z_j(\Phi_j^0(x) + \Psi^{ext,*}(x)),$$

$$\mathbf{j}_j(x) = \frac{z_j}{\mathrm{Pe}_j|Y_F|}\int_{Y_F} n_j^0(y)(\nabla_x\Phi_j^0(x) + \mathbf{E}^* + \nabla_y\Phi_j^1(x,y) + \frac{\mathrm{Pe}_j}{z_j}\mathbf{u}^0(x,y))dy,$$

$$\mathbf{u}(x) = \frac{1}{|Y_F|}\int_{Y_F}\mathbf{u}^0(x,y)\,dy.$$

From Eqs. 59–61, we deduce the homogenized or upscaled equations for the above effective fields.

Proposition 5 [3] *Introducing the flux* $\mathcal{J}(x) = (\mathbf{u}, \{\mathbf{j}_j\}_{1\le j\le N})$ *and the gradient* $\mathcal{F}(x) = (\nabla_x p^0, \{\nabla_x\mu_j\}_{1\le j\le N})$, *the macroscopic equations are*

$$\mathrm{div}_x\,\mathcal{J} = 0 \quad in\ \ \Omega, \tag{62}$$

$$\mathcal{J} = -\mathcal{M}\mathcal{F} - \mathcal{M}(\mathbf{f}^*, \{0\}) \tag{63}$$

with a symmetric positive definite $\mathcal{M}$, *defined by*

$$\mathcal{M} = \begin{pmatrix} \mathbb{K} & \frac{\mathbb{J}_1}{z_1} & \cdots & \frac{\mathbb{J}_N}{z_N} \\ \mathbb{L}_1 & \frac{\mathbb{D}_{11}}{z_1} & \cdots & \frac{\mathbb{D}_{1N}}{z_N} \\ \vdots & \vdots & \ddots & \vdots \\ \mathbb{L}_N & \frac{\mathbb{D}_{N1}}{z_1} & \cdots & \frac{\mathbb{D}_{NN}}{z_N} \end{pmatrix}, \tag{64}$$

and complemented with periodic boundary conditions for p^0 *and* $\{\Phi_j^0\}_{1\le j\le N}$. *The matrices* $\mathbb{J}_i$, $\mathbb{K}$, $\mathbb{D}_{ji}$ *and* $\mathbb{L}_j$ *are defined by their entries*

$$\{\mathbb{J}_i\}_{lk} = \frac{1}{|Y_F|}\int_{Y_F}\mathbf{v}^{i,k}(y)\cdot\mathbf{e}^l\,dy,$$

$$\{\mathbb{K}\}_{lk} = \frac{1}{|Y_F|}\int_{Y_F}\mathbf{v}^{0,k}(y)\cdot\mathbf{e}^l\,dy,$$

$$\{\mathbb{D}_{ji}\}_{lk} = \frac{1}{|Y_F|}\int_{Y_F} n_j^0(y)\left(\mathbf{v}^{i,k}(y) + \frac{z_j}{\mathrm{Pe}_j}\left(\delta_{ij}\mathbf{e}^k + \nabla_y\theta_j^{i,k}(y)\right)\right)\cdot\mathbf{e}^l\,dy,$$

$$\{\mathbb{L}_j\}_{lk} = \frac{1}{|Y_F|}\int_{Y_F} n_j^0(y)\left(\mathbf{v}^{0,k}(y) + \frac{z_j}{\mathrm{Pe}_j}\nabla_y\theta_j^{0,k}(y)\right)\cdot\mathbf{e}^l\,dy.$$

Remark 6 The tensor $\mathbb{K}$ is called permeability tensor, $\mathbb{D}_{ji}$ are the electrodiffusion tensors. The symmetry of the tensor $\mathcal{M}$ is equivalent to the famous Onsager's reciprocal relations. It was already proved in [26]. However, the positive definiteness of $\mathcal{M}$ was proved in [3]. It is essential in order to state that Eqs. 62–63 is an elliptic system which admits a unique solution.

The closeness of the solution to the homogenized problem, to the solution of the original problem is given by the following result.

Theorem 7 [3] *Let* $(p^0, \{\Phi_j^0\}_{1\le j\le N})$ *be defined by Eqs.* 62 and 63. *Let* $\mathbf{u}^0$ *be given by Eq.* 59 *and* $\{\Phi_j^1\}_{1\le j\le N}$ *by Eq.* 61. *Then in the limit* $\varepsilon \to 0$ *we have*

$$\int_{\Omega^\varepsilon} \left(\left| \mathbf{u}^\varepsilon(x) - \mathbf{u}^0\left(x, \frac{x}{\varepsilon}\right)\right|^2 + |P^\varepsilon(x) - p^0(x)|^2 \right) dx \to 0 \tag{65}$$

and

$$\int_{\Omega^\varepsilon} \left| \nabla \left(\Phi_j^\varepsilon(x) - \Phi_j^0(x) - \varepsilon \Phi_j^1\left(x, \frac{x}{\varepsilon}\right)\right)\right|^2 dx \to 0. \tag{66}$$

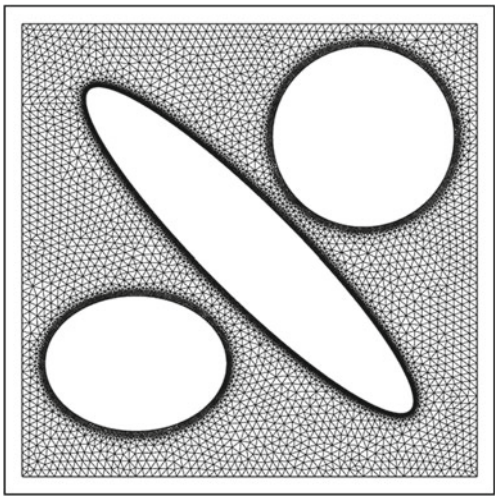

Fig. 1 Mesh for a periodicity cell with ellipsoidal inclusions

4 Numerical study of the effective tensor

We now present some numerical tests in the two-dimensional case obtained with the *FreeFem++* package [39]. The linearization of the ionic transport equations allows us to decouple the computation of the electrostatic potential from those of the cell problems. First, we compute Ψ^0, solution of Eq. 34, from which we infer the concentrations $n_j^0(y) = n_j^c \exp\{-z_j \Psi^0(y)\}$. Second, knowing the n_j^0's which are coefficients for the cell problems 51–53 and 55–58, we compute their solutions. Finally, we evaluate the various entries of the effective tensor (Eq. 64) according to the formula from Proposition 5. In all figures, we plot the adimensionalized entries of the effective tensors (Eq. 64). However, when the concentrations are involved, we plot them in their physical units, namely we use the dimensional quantity

$$n_j^0(\infty) = n_c\, n_j^c. \tag{67}$$

For solving the highly nonlinear Poisson–Boltzmann equation, we use Lagrange P2 finite elements and a Newton–Raphson algorithm. We also rely on a special feature of mesh adaptivity available in FreeFem++ for automatic mesh refinement in order to achieve a good numerical precision. Since in most cases, the electrostatic potential is varying as a boundary layer close to the solid boundaries, our meshes are much refined close to those boundaries (see e.g., Fig. 1). More precisely, the mesh is adapted for the initialization of the Newton algorithm which amounts to solve the linear Debye–Hückel model. Once the mesh has been refined during this initialization step, it stays the same for all further Newton iterations (the same mesh is also used for solving the cell problems). The total number of degrees of freedom is around 10,000 (depending on the infinite dilution concentration n_j^c).

All the following computations are conducted for an aqueous solution of *NaCl* at 298 K (Kelvin), where species $j = 1$ is the cation Na^+ ($z_1 = 1$) with diffusivity $D_1^0 = 13.33\text{e}{-10}\,\text{m}^2/\text{s}$ and species $j = 2$ the anion Cl^- ($z_2 = -1$) with $D_2^0 = 20.32\text{e}{-10}\,\text{m}^2/\text{s}$. The infinite dilution concentrations of the species are considered equal, $n_1^c = n_2^c$, and the characteristic concentration is $n_c = 0.1\text{mol/l}$. The dynamic viscosity η is equal to $0.89\text{e}{-3}\,\text{kg/(m sec)}$. Instead of using the formula of Table 1 for defining the Debye length, we use the following definition

$$\lambda_D = \sqrt{\frac{\mathcal{E} k_B T}{e^2 \sum_{j=1}^N n_j z_j^2}}$$

which differs by a factor of $\sqrt{2}$ in the present case of two monovalent ions. Other physical values are to be found in Table 1. Two model geometries are considered in this section. The first one features ellipsoid solid inclusions (see Fig. 1) which allows us to perform variations of concentrations from 10^{-3} to 1mol/l and variations of the pore size ($3 \le \ell \le 50$ nm). Even if the model represents an idealized geological porous media, it is not far from real montmorillonite clays made of ellipsoidal tactoids whose dimension is between 35 and 400 nm long [8]. The second one is a rectangular model (see Fig. 2) which allows us to perform porosity variation. The goal of this section is to study the variations of the effective tensor according to these parameters (concentration, pore size, and porosity).

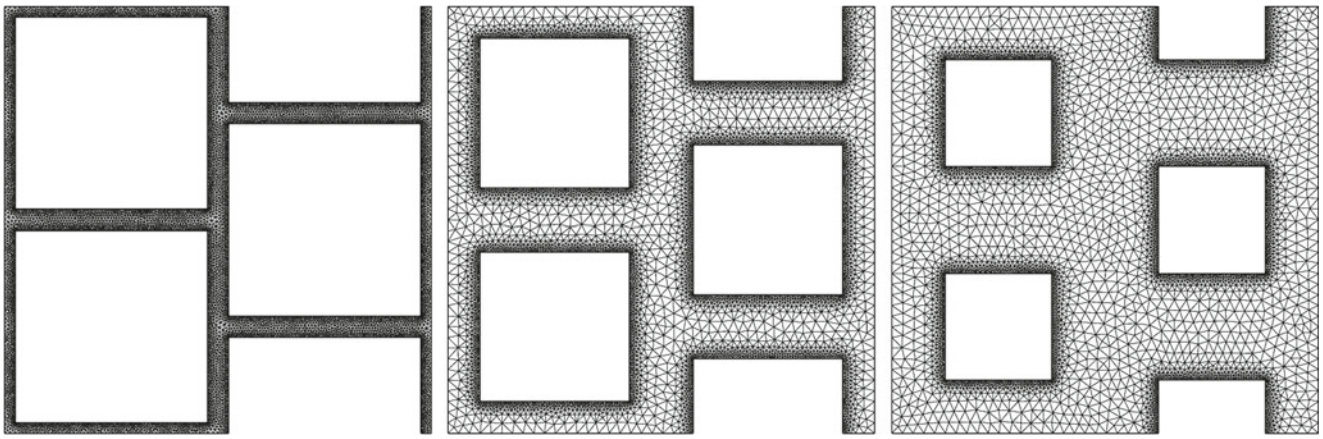

Fig. 2 Meshes for three different porosities (0.19, 0.51, and 0.75) of a periodic cell with rectangular inclusions

4.1 Variation of the concentration

For the geometry with ellipsoidal inclusions, we vary the infinite dilution concentrations n_j^c in the range $(10^{-2}, 10)$ or, equivalently through Eq. 67, the dimensional infinite dilution concentrations $n_j^0(\infty)$ varies from 10^{-3} to 1 mol/l. The pore size is $\ell = 50$ nm. Varying proportionally all values of n_j^c is equivalent to varying the parameter β in the Poisson–Boltzmann Eq. 34. Therefore, low values of n_j^c correspond to the limit problem 39 for the electrostatic potential Ψ^0, while large values of n_j^c correspond to the asymptotic limit behavior (Eq. 35) (for which the concentrations $n_j^0(y)$ are constant, at electroneutral equilibrium, away from the boundary). As can be checked on Fig. 3, varying n_j^c is equivalent to varying the cell-average of the concentrations $|Y_F|^{-1} \int_{Y_F} n_j(y)\, dy$ (at least away from very small concentrations) since our numerical results show that they depend almost linearly on each other. However, in full mathematical rigor, the concentration $n_j(y)$ does not depend linearly on n_j^c. Indeed, formula 33 states that $n_j^0(y) = n_j^c \exp\{-z_j \Psi^0(y)\}$ and Ψ^0 depends on n_j^c too, through the Poisson–Boltzmann Eq. 34.

As explained in Remark 4, when β is large, or equivalently when the infinite dilution concentrations n_j^c are large, the cell problems 51–52 and 55–56 become identical to the usual Stokes cell problems which give the formula for the usual permeability tensor [20, 45]. Therefore, it makes sense to divide all entries of the permeability tensor $\mathbb{K}$ by the corresponding ones for a pure filtration problem (this renormalization avoids any spurious dependence on the pore size ℓ). The resulting relative permeability coefficients are plotted on Fig. 4: the smaller the infinite dilution concentration, the smaller the permeability. We clearly see an asymptotic limit of the relative permeability tensor not only for high concentrations (i.e., Debye length smaller than the pore size $\beta \to \infty$) but also for low concentrations (i.e., Debye length larger than the pore size $\beta \to 0$). In

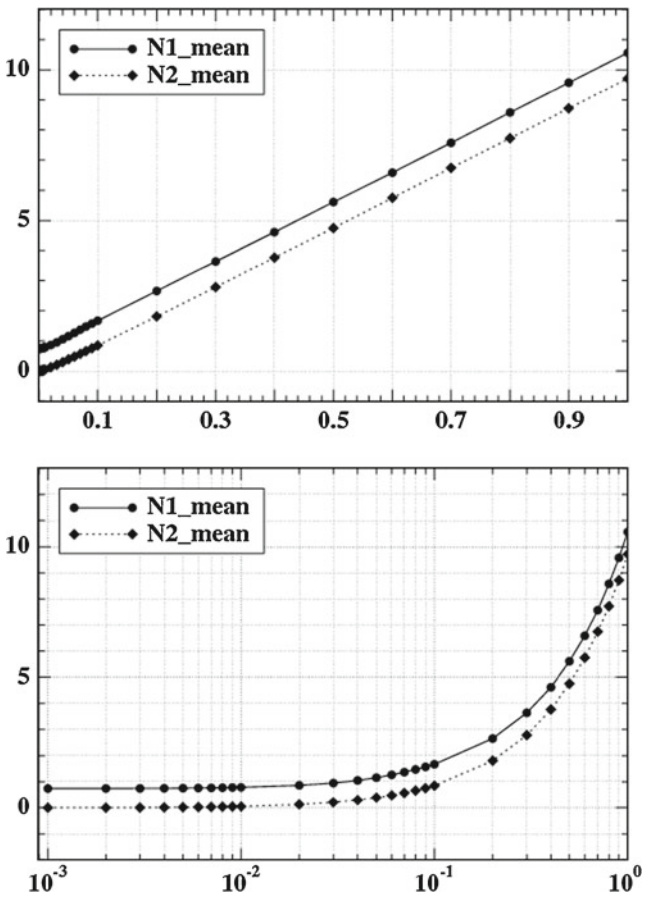

Fig. 3 Averaged cell concentration $\text{Nj\_mean} = |Y_F|^{-1} \int_{Y_F} n_j(y)\, dy$ as a function of the dimensional (in mole per liter) infinite dilution concentrations $n_j^0(\infty)$: normal scale (*top*) and semi-log scale (*bottom*)

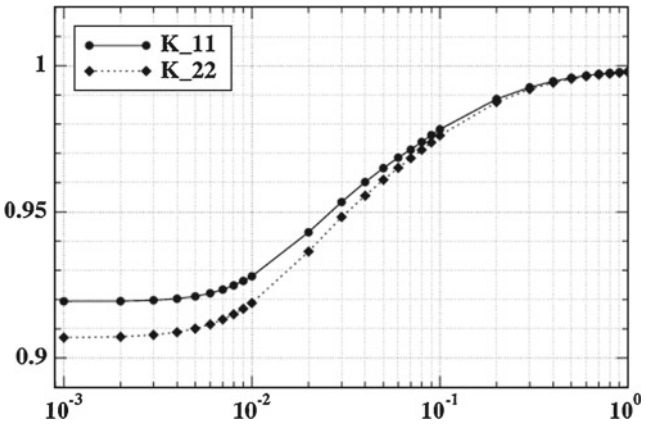

Fig. 4 Diagonal entries of the relative permeability tensor, $\mathbb{K}_{11}$ and $\mathbb{K}_{22}$, as functions of the dimensional (in mole per liter) infinite dilution concentrations $n_j^0(\infty)$

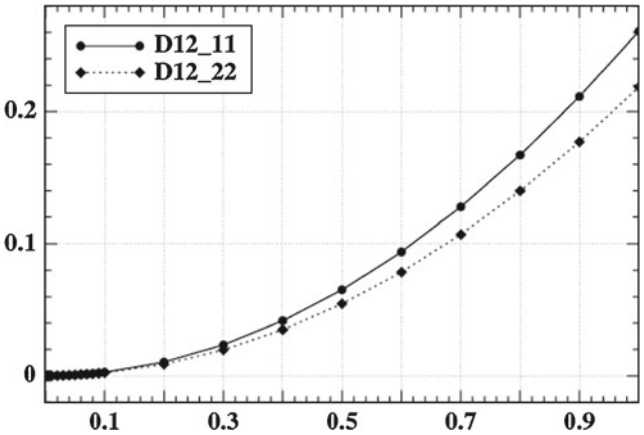

Fig. 6 Diagonal entries of the cross-diffusion tensor $\mathbb{D}_{12}$, as functions of the dimensional (in mole per liter) infinite dilution concentrations $n_j^0(\infty)$

the latter regime, the hydrodynamic flux is reduced: the electrostatic attraction of the counterions with respects to the surface slows down the fluid motion. This effect is not negligible because the Debye layer is important.

On Fig. 5, we plot the entries of the electrodiffusion tensor $\mathbb{D}_{11}$ for the cation. A similar behavior is obtained for the other tensor $\mathbb{D}_{22}$ for the anion. As expected, the flux increases with the infinite dilution concentration n_j^c. It is not a linear law because even at low concentration, there are still counterions; they do not appear to be very mobile, though. The cross-diffusion tensor $\mathbb{D}_{12}$ is displayed on Fig. 6: for large concentrations, it is of the same order of magnitude than the species diffusion tensors $\mathbb{D}_{11}$ and $\mathbb{D}_{22}$, because of the strong electrostatic interactions between the ions. A mathematical asymptotic analysis (similar to that in Remark 4) shows that the electrodiffusion tensors $\mathbb{D}_{ji}$ behaves quadratically as a function of n_j^c when n_j^c becomes very large. This asymptotic behavior is clearly seen on Fig. 7 where the slope of the curve is approximately 2.

The coupling tensors $\mathbb{L}_1$ and $\mathbb{L}_2$ are plotted on Fig. 8. The coupling is, of course, maximal for large concentrations but the coupling tensor $\mathbb{L}_1$ for the cation does not vanish for very small infinite dilution concentrations since the cell-average of the cation concentration has a nonzero limit (required to compensate the negative surface charge) as can be checked on Fig. 3.

4.2 Variation of pore size

We now vary the pore size ℓ for the same geometry with ellipsoidal inclusions. Varying ℓ is equivalent to vary the parameter β, defined by Eq. 12, in the Poisson–Boltzmann Eq. 34. It thus changes the values

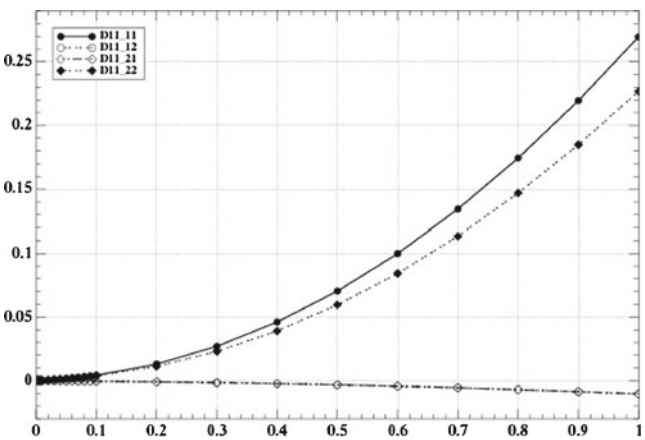

Fig. 5 Entries of the electrodiffusion tensor $\mathbb{D}_{11}$ for the cation, as functions of the dimensional (in mole per liter) infinite dilution concentrations $n_j^0(\infty)$

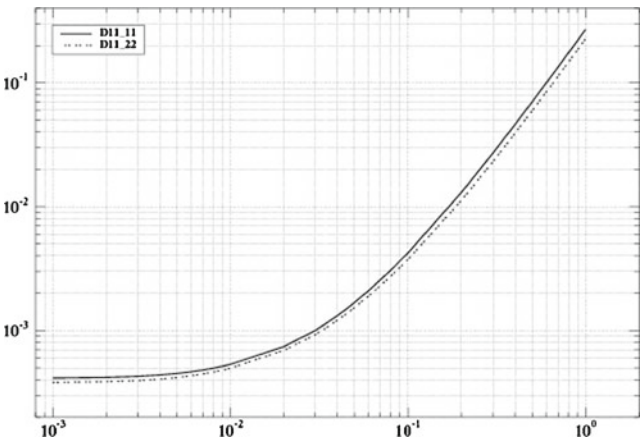

Fig. 7 Diagonal entries of the electrodiffusion tensor $\mathbb{D}_{11}$ as functions of the dimensional (in mole per liter) infinite dilution concentrations $n_j^0(\infty)$ (log-log plot)

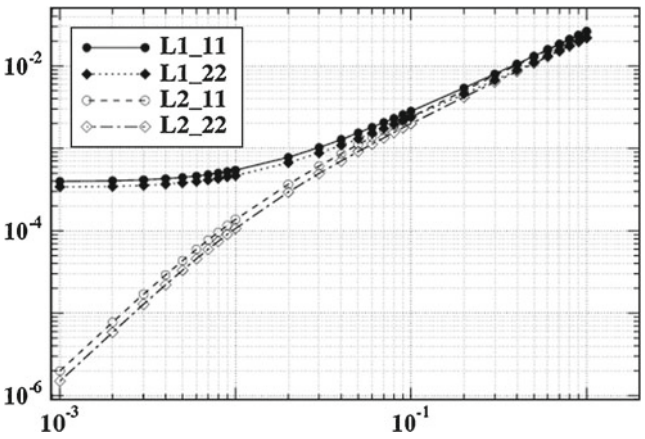

Fig. 8 Diagonal entries of the coupling tensors $\mathbb{L}_1$ and $\mathbb{L}_2$, as functions of the dimensional (in mole per liter) infinite dilution concentrations $n_j^0(\infty)$ (log-log plot)

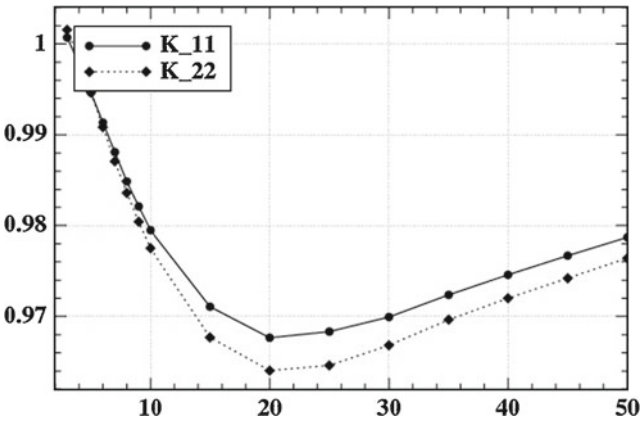

Fig. 10 Relative permeability coefficients $\mathbb{K}_{11}$ and $\mathbb{K}_{22}$ versus pore size ℓ (in nanometer)

of the local concentrations $n_j^0(y)$ in the definition of the cell problems (51–54) and (55–58): this is the only modification which is brought into the cell problems. On Fig. 9, we plot the electrostatic potential Ψ^0, solution of the Poisson–Boltzmann Eq. 34, for small and large values of β. As predicted by the asymptotic analysis of Section 2.3, for large β, the potential Ψ^0 behaves like a boundary layer and is almost constant, equal to zero, away from the pore walls.

On Fig. 10, we plot the relative permeability coefficients with respect to the ones of the Stokes problem. Surprisingly, the variation is not monotone and there seems to be a minimum for a pore size of 20 nm. This is the signature of a transition from a bulk diffusion regime for small pores to a surface diffusion regime (caused by the charged boundaries) at large pores. Globally, the counterions reduce the hydrodynamic flow because of the attraction with the surface, but this relaxation effect is less important at very large or very small pore size l. More precisely, if the pore size becomes very large, the electrostatic screening is important, as already mentioned. Thus the domain of attraction becomes very small and the lowering of the hydrodynamic flow is reduced: the permeability is increased. On the other hand, for very small pores, the counterion profile becomes more and more uniform. Consequently, there is no screening, but the hydrodynamic flow does not modify a lot the counterion distribution, since it is globally uniform and the resulting electrostatic slowdown becomes less important.

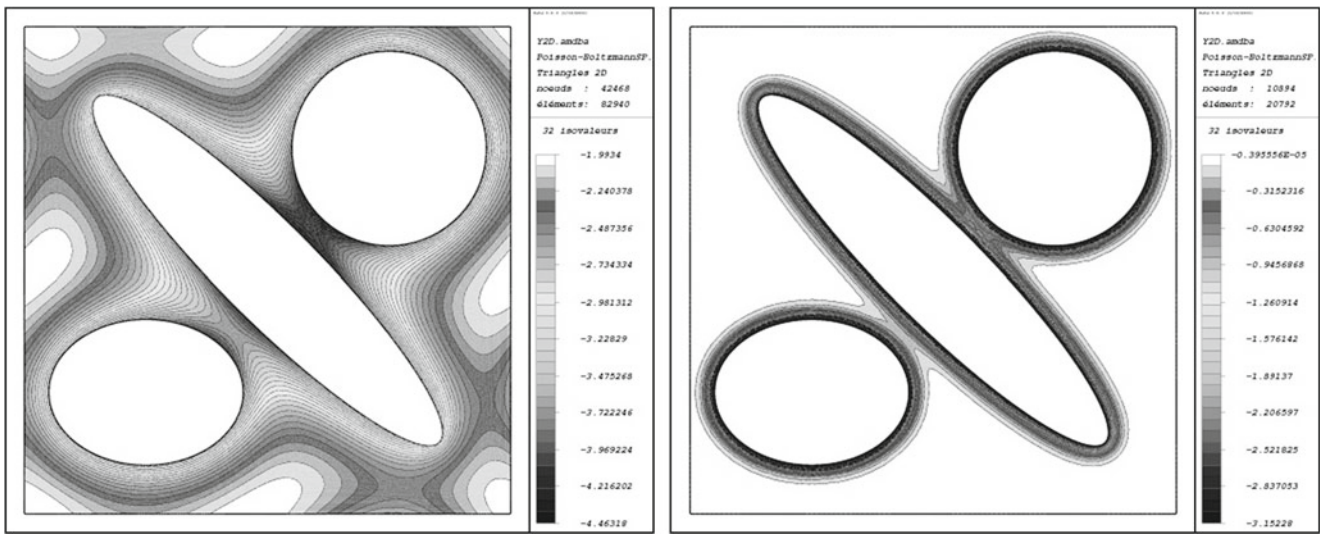

Fig. 9 Electrostatic potential Ψ^0, solution of the Poisson–Boltzmann Eq. 34, for a pore size $\ell = 3$ nm (*left*) and $\ell = 50$ nm (*right*)

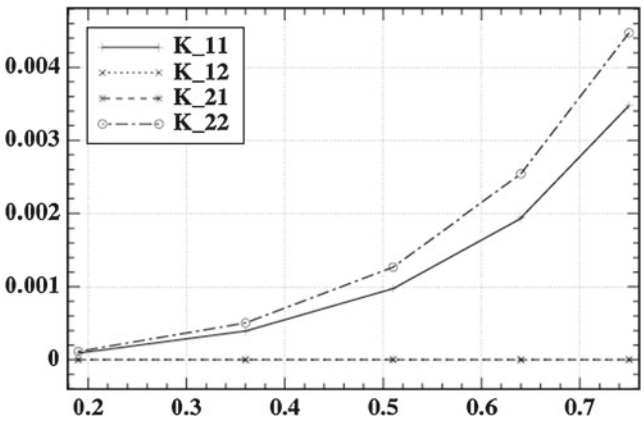

Fig. 11 Permeability tensor $\mathbb{K}$ versus porosity ($n_j^0(\infty) = 0.1$ mol/l)

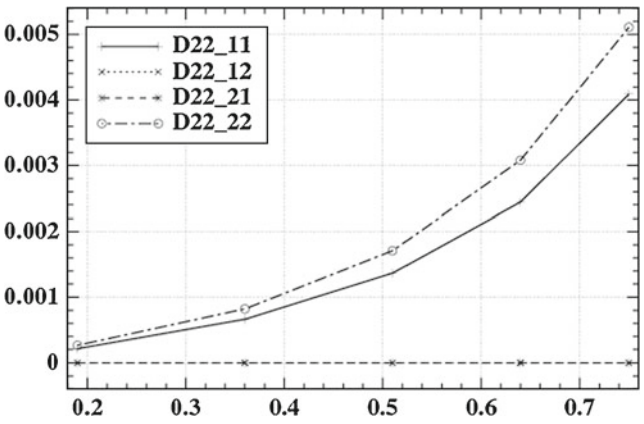

Fig. 13 Electrodiffusion tensor $\mathbb{D}_{11}$ for the cation versus porosity ($n_j^0(\infty) = 0.1$ mol/l)

4.3 Variation of the porosity

Eventually, we investigate the influence of the porosity on the effective tensors. To this end, we rely on the rectangular geometry where we vary the size of the inclusions (see Fig. 2). The infinite dilution concentration is fixed at $n_j^c = 1$, or $n_j^0(\infty) = 0.1 mol/l$. The porosity is defined as $|Y_F|/|Y|$ and takes the successive values of 0.19, 0.36, 0.51, 0.64, and 0.75 in our computations. On Fig. 11, we check that the permeability tensor is increasing with porosity, as expected. The same happens for the electrodiffusion tensor $\mathbb{D}_{22}$ for the anion on Fig. 12. More surprising is the behavior of the electrodiffusion tensor $\mathbb{D}_{11}$ for the cation on Fig. 13: again there is a minimum value attained for a 0.35 value of the porosity. This may be explained again by a transition from a bulk diffusion regime for large porosities to a surface diffusion regime (caused by the charged boundaries) for small porosities.

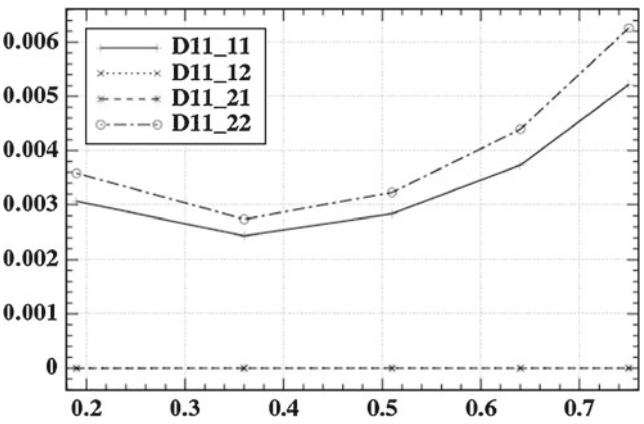

Fig. 12 Electrodiffusion tensor $\mathbb{D}_{22}$ for the anion versus porosity ($n_j^0(\infty) = 0.1$ mol/l)

5 Conclusion

In this article, we presented a homogenization method for upscaling the electrokinetic equations. We obtained the homogenized system (62–63) which can be rewritten in dimension form, for the effective unknowns $p^{eff} = p_c p^0$ and $\Phi_i^{eff} = \frac{k_B T}{e}\Phi_i^0$, and for $1 \le j \le N$, as

$$\mathrm{div}_x \left\{ \frac{\mathbb{K}\ell^2}{\eta}(\nabla_x p^{eff} + \mathbf{f}) + \sum_{i=1}^{N} \frac{\mathbb{J}_i \ell^2 n_c e}{\eta} \times (\nabla_x \Phi_i^{eff} + \mathbf{E}) \right\} = 0 \ \text{ in } \ \Omega, \tag{68}$$

$$\mathrm{div}_x \left\{ \frac{\mathbb{L}_j\ell^2}{\eta}(\nabla_x p^{eff} + \mathbf{f}) + \sum_{i=1}^{N} \frac{\mathbb{D}_{ji} \ell^2 n_c e}{\eta} \times (\nabla_x \Phi_i^{eff} + \mathbf{E}) \right\} = 0 \ \text{ in } \ \Omega. \tag{69}$$

We computed the homogenized or effective tensors for several geometric configurations and a large range of physical parameters.

Some conclusions come out naturally from our analytical and numerical results:

- Relative permeability is maximal for very small pores. It first decreases and then increases as the pore size is increasing (see Fig. 10).
- Permeability is, of course, increasing as a function of porosity (see Fig. 11).
- Permeability is increasing as a function of the infinite dilution concentration (see Fig. 4). The qualitative analysis from Section 2.3 is confirmed by our numerical simulations.

- The diagonal entries of the electrodiffusion tensor are monotone increasing with respect to all parameters, except possibly porosity.

Our asymptotic analysis of the Poisson–Boltzmann equation for small/large concentrations and small/large pores seems to be new in the case of Neumann conditions (given surface charges). Although previous results were obtained for Dirichlet conditions (given surface potential) [17], the limits for Neumann or Dirichlet boundary conditions are not the same. In our case, in the limit $\beta \to 0$, only one type of ion matters in the charge density.

The proposed homogenized model contributes to the understanding of effective electrokinetic flows through Onsager's relations. We give a systematic method of calculating the permeability and the electrodiffusion tensor, which can be used not only for periodic media but also for random statistically homogeneous porous media.

Acknowledgements This research was partially supported by the GNR MOMAS CNRS-2439 (Modélisation Mathématique et Simulations numériques liées aux problèmes de gestion des déchets nucléaires) (PACEN/CNRS, ANDRA, BRGM, CEA, EDF, IRSN) and GNR PARIS (Propriétés des actinides et des radionucléides aux interfaces et aux solutions). The authors would like to thank O. Bernard, V. Marry, B. Rotenberg and P. Turq from the Modélisation et Dynamique Multi-échelles team from the laboratory Physicochimie des Electrolytes, Colloïdes et Sciences Analytiques (PECSA), UMR CNRS 7195, Université P. et M. Curie, for helpful discussions. G.A. is a member of the DEFI project at INRIA Saclay Ile-de-France. G.A. is partially supported by the Chair "Mathematical modelling and numerical simulation, F-EADS – Ecole Polytechnique – INRIA."

References

1. Adler, P., Mityushev, V.: Effective medium approximation and exact formulae for electrokinetic phenomena in porous media. J. Phys. A: Math. Gen. **36**, 391–404 (2003)
2. Allaire, G., Dufrêche, J.-F., Mikelić, A., Piatnitski, A.: Asymptotic analysis of the Poisson–Boltzmann equation describing electrokinetics in porous media. Nonlinearity **26**, 881–910 (2013)
3. Allaire, G., Mikelić, A., Piatnitski, A.: Homogenization of the linearized ionic transport equations in rigid periodic porous media. J. Math. Phys. **51**,123103 (2010). doi:10.1063/1.3521555
4. Auriault, J.-L., Strzelecki, T.: On the electro-osmotic flow in a saturated porous medium. Int. J. Eng. Sci. **19**, 915-928 (1981)
5. Barcilon, V., Chen, D.-P., Eisenberg, R.S., Jerome, J.W.: Qualitative properties of steady-state Poisson–Nernst–Planck systems: perturbation and simulation study. SIAM J. Appl. Math. **57**(3), 631–648 (1997)
6. Benco, L., Tunega, D., Hafner, J., Lischka, H.: Ab initio density functional theory applied to the structure and proton dynamics of clays. Chem. Phys. Lett. **333**, 479 (2001)
7. Bensoussan, A., Lions, J.L., Papanicolaou, G.: Asymptotic analysis for periodic structures. In: Studies in Mathematics and its Applications, vol. 5. North-Holland Publishing Co., Amsterdam (1978)
8. Cadene, A., Durand-Vidal, S., Turq, P., Brendle, J.: Study of individual Na-montmorillonite particles size, morphology, and apparent charge. J. Colloid Interface Sci. **285**, 719–730, (2005)
9. Chan, D.Y., Horn, R.G.: The drainage of thin liquid films between solid surfaces, J. Chem. Phys. **83**, 5311–5325 (1985)
10. Coelho, D., Shapiro, M., Thovert, J.F., Adler, P.: Electro-osmotic phenomena in porous media. J. Colloid Interface Sci. **181**, 169–90 (1996)
11. Dormieux, L., Lemarchand, E., Coussy, O.: Macroscopic and micromechanical approaches to the modelling of the osmotic swelling in clays. Transp. Porous Media **50**, 75–91 (2003)
12. Dufrêche, J.-F., Bernard, O., Durand-Vidal, S., Turq, P.: Analytical theories of transport in concentrate electrolyte solutions from the msa. J. Phys .Chem. B **109**, 9873 (2005)
13. Dufrêche, J.-F., Marry, V., Malikova, N., Turq, P.: Molecular hydrodynamics for electro-osmosis in clays: from Kubo to Smoluchowski. J. Mol. Liq. **118**, 145 (2005)
14. Edwards, D.A.: Charge transport through a spatially periodic porous medium: electrokinetic and convective dispersion phenomena. Philos. Trans. R. Soc. Lond. A **353**, 205–242 (1995)
15. Greathouse, J.A., Refson, K., Sposito, G.M.: Molecular dynamics simulation of water mobility in magnesium-smectite hydrates. J. Am. Chem. Soc. **122**, 11459 (2000)
16. de Groot, S.R., Mazur, P.: Non-equilibrium Thermodynamics. North-Holland, Amsterdam (1969)
17. Gupta, A.K., Coelho, D., and Adler, P.: Electroosmosis in porous solids for high zeta potentials, J Colloid Interface Sci. **303**, 593–603 (2006)
18. Gupta, A.K., Coelho, D., Adler, P.: Ionic transport in porous media for high zeta potentials, J Colloid Interface Sci. **314**, 733–747 (2006)
19. Hansen, J.-P., Löwen, H.: Effective interactions between electrical double layers. Ann. Rev. Phys. Chem. **51**, 209 (2000)
20. Hornung, U. ed.: Homogenization and porous media. In: Interdisciplinary Applied Mathematics, vol. 6. Springer-Verlag, New York (1997)
21. Karaborni, S., Smit, B., Heidung, W., Urai, J., van Oort, E.: The swelling of clays: simulation of the hydration of montmorillonite. Science **271**, 1102 (1996)
22. Karniadakis, G., Beskok, A., Aluru, N.: Microflows and nanoflows. Fundamentals and simulation. In: Interdisciplinary Applied Mathematics, vol. 29. Springer, New York (2005)
23. Leroy, P., Revil, A.: A triple layer model of the surface electrochemical properties of clay minerals. J. Colloid Interface Sci **270**, 37 (2004)
24. Lions, J.-L.: Some Methods in the Mathematical Analysis of Systems and their Controls. Science Press, Beijing, Gordon and Breach, New York (1981)
25. Looker, J.R.: Semilinear elliptic Neumann problems and rapid growth in the nonlinearity. Bull. Aust. Math. Soc. **74**(2), 161–175 (2006)
26. Looker, J.R., Carnie, S.L.: Homogenization of the ionic transport equations in periodic porous media. Transp. Porous Media **65**, 107–131 (2006)
27. Lyklema, J.: Fundamentals of Interface and Colloid Science, vol 2. Academic (1995)
28. Malikova, N., Marry, V., Dufrêche, J.-F., Turq, P.: Temperature effect in a montmorillonite clay at low hydration-microscopic simulation. Mol. Phys. **102**, 1965 (2004)

29. Marino, S., Shapiro, M., Adler, P.: Coupled transports in heterogeneous media, J. Colloid Interface Sci. **243**, 391–419 (2001)
30. Marry, V., Dufrêche, J.-F., Jardat, M., Turq, P.: Equilibrium and electrokinetic phenomena in charged porous media from microscopic and mesoscopic models: electro-osmosis in montmorillonite. Mol. Phys. **101**, 3111 (2003)
31. Marry, V., Turq, P.: Microscopic simulations of interlayer structure and dynamics in bihydrated heteroionic montmorillonites. J. Phys. Chem. B **107**, 183 (2003)
32. Moyne, C., Murad, M.: Electro-chemo-mechanical couplings in swelling clays derived from a micro/macro-homogenization procedure. Int. J. Solids Struct. **39**, 6159–6190 (2002)
33. Moyne, C., Murad, M.: Macroscopic behavior of swelling porous media derived from micromechanical analysis. Transp. Porous Media **50**, 127–151 (2003)
34. Moyne, C., Murad, M.: A Two-scale model for coupled electro-chemomechanical phenomena and Onsager's reciprocity relations in expansive clays: I Homogenization analysis. Transp. Porous Media **62**, 333–380 (2006)
35. Moyne, C., Murad, M.: A two-scale model for coupled electro-chemo-mechanical phenomena and Onsager's reciprocity relations in expansive clays: II. computational validation. Transp. Porous Media **63(1)**, 13–56 (2006)
36. Moyne, C., Murad, M.: A dual-porosity model for ionic solute transport in expansive clays. Comput. Geosci. **12**, 47–82 (2008)
37. O'Brien, R.W., White, L.R.: Electrophoretic mobility of a spherical colloidal particle. J. Chem. Soc. Faraday Trans. **2**(74), 1607–1626 (1978)
38. Park, J.-H., Jerome, J.W.: Qualitative properties of steady-state Poisson–Nernst–Planck systems: mathematical study. SIAM J. Appl. Math. **57**(3), 609–630 (1997)
39. Pironneau, O., Hecht, F., Le Hyaric, A.: FreeFem++ version 3.20. http://www.freefem.org/ff++ (2012)
40. Ray, N., Ch. Eck, Muntean, A., Knabner, P.: Variable choices of scaling in the homogenization of a Nernst–Planck–Poisson problem. Institut für Angewandte Mathematik, Universitaet Erlangen-Nürnberg (2011) (Preprint no. 344)
41. Ray, N., Muntean, A., Knabner, P.: Rigorous homogenization of a Stokes–Nernst–Planck–Poisson system. J. Math. Anal. Appl. **390**, 374–393 (2012)
42. Ray, N., van Noorden, T., Frank, F., Knabner, P.: Multiscale modeling of colloid and fluid dynamics in porous media including an evolving microstructure. Transp. Porous Media **95**, 669–696 (2012)
43. Rosanne, M., Paszkuta, M., Adler, P.: Electrokinetic phenomena in saturated compact clays. J Colloid Interface Sci. **297**, 353–364 (2006)
44. Rosanne, M., Paszkuta, M., Thovert, J.F., Adler, P.: Electro-osmotic coupling in compact clays. Geophys. Res. Lett. **31**, L18614 (2004)
45. Sanchez-Palencia, E.: Nonhomogeneous media and vibration theory. In: Lecture Notes in Physics, vol. 127. Springer-Verlag, Berlin (1980)
46. Schmuck, M.: Modeling and deriving porous media Stokes–Poisson–Nernst–Planck equations by a multiple-scale approach. Commun. Math. Sci. **9**, 685–710 (2011)
47. Schmuck, M.: First error bounds for the porous media approximation of the Poisson–Nernst–Planck equations. ZAMM Z. Angew. Math. Mech. **92**, 304–319 (2012)
48. Skipper, N.T., Sposito, G., Chang, F.-R.C.: Monte Carlo simulation of interlayer molecular structure in swelling clay minerals; 2, monolayer hydrates. Clays Clay Miner. **43**, 294 (1995)
49. Trizac, E., Bocquet, E.L., Weiss, J.J., Aubouy, M.: Effective interactions and phase behaviour for a model clay suspension in an electrolyte. J. Phys. Condens. Matter **122**, 11459 (2000)
50. Tunega, D., Gerzabek, M.H., Lischka, H.: Ab initio molecular dynamics study of a monomolecular water layer on octahedral and tetrahedral kaolinite surfaces. J. Phys. Chem. B **108**, 5930 (2004)